The SAR map-drift algorithm extended for a multi-hydrophone SAS

P. T. Gough and M. A. Miller,
Acoustics Research Group, Department of Electrical and Computer Engineering,
University of Canterbury, Private Bag 4800, Christchurch, New Zealand.
Email:p.gough@elec.canterbury.ac.nz Phone:[+64] 3 364 2297

Abstract—**The problems caused by random sway errors in the tow-path of a single hydrophone, synthetic aperture sonar (SAS) are well- known. If these horizontal displacement errors are left uncorrected and the tow- path is assummed to be straight, they have a devasting effect on the quality of the reconstructed image. Although on-board navigation instruments can help measure the gross departures from the straight path, sub-wavelength residual sway errors still corrupt the imaging process. An early sway estimation technique in SAR (called the map-drift algorithm) was to divide the full aperture up into two equal, but non-overlapping, sub-apertures. By cross-correlating the resultant two low- resolution images, an estimate of the equivalent phase error (that is the sway error divided by the wavelength and multiplied by π) could be obtained for the second order coefficient of the polynomial describing the sway between the images the two-image map-drift algorithm could be extended to smaller and smaller sub- apertures with the phase error estimated to higher and higher orders of the polynomial. The limit of the method is when the subaperture images are of such a low resolution that it is not possible to detect the differential sway between adjacent images. More recently SAS systems have a single transmitter +projector and an array of receiving hydrophones so that the echoes received from any one ping can be reconstructed into a low-resolution image centred on the rotational axis of the real array. The images from adjacent pings are cross-correlated to determine how the sonar has moved between pings. The sub-aperture (cf. map-drift algorithm) is thus determined by the extent of the physical array. From the cross-correlation, the differential sway can be estimated from a series of displaced single ping images just as in the map-drift algorithm. By measuring the rotational displacement between images we can also estimate the relative yaw between single ping images. Using simulated, distorted SAS data as input, the proposed DPIA algorithm shows promise in that it can estimate yaw with sufficient accuracy to restore distorted SAS images very close to their diffraction-limit. Here we present "before and after" simulated images from an extant SAS and demonstrate the power (and also the limitations) of the proposed DPIA technique.**

I. Introduction

Any synthetic aperture sonar (SAS), whether based on a single-receiver or multiple-receiver system, is limited by the uncorrected random motion of the tow-fish [1], [2], [3], [4]. Although there are three translational displacement and three rotational degrees of freedom in a free body, only sway (side-to-side horizontal displacement from the mean tow-path) and yaw (horizontal angular variation around the average direction of travel) are considered important for non-bathymetric, side-scan sonar imaging. In shallow waters where SAS has significant advantages over traditional side-scan sonars, a single-receiver SAS is mostly effected by sway. However, a multiple receiver SAS is effected by yaw as well as by sway. Currently available on-board navigation instruments are unable to measure all of the motion errors to the accuracy required, so we also need some additional autofocus (aka "micro-navigation") techniques, based on analysis of the recorded data, to estimate the actual yaw and sway used for complete correction of all random motion. Since all future SAS systems are likely to use a single transmitter coupled with a multiple-receiver linear array, it makes sense to estimate the critical motion parameters of yaw and sway together rather than only one or the other.

So far these two critical motion parameters have been estimated by applying an autofocussing technique variously known as the "Displaced Phase Center Antenna" (DPCA), "Displaced Phase Center" (DPC) autofocus [5] or "Redundant Phase Center" (RPC) autofocus [6]. The RPC technique requires the multi-hydrophone SAS to travel down the track slower than its maximum allowable speed (as determined from the along-track spatial sampling criteria). For each transmitted ping, an ensemble of bistatic transmitter/receiver pairs is created. The position of the (single) transmitter is different from the position of any individual receiver in the along-track array. However, the returns from each bistatic transmitter-receiver pair can be approximated by those from an equivalent number of monostatic transmitter-receiver sonars placed at a median locations of each pair. The median location is called the **phase centre** of the pair. At less than maximum speed, the forward-most phase centers of the first ping overlap the rear-most phase centers of the second ping and there is high degree of redundancy between the unprocessed echo returns from the near co-located phase centers. What is important is that the medium is stable (i.e. there is good temporal correlation between pings) so any phase and time shifts in the cross correlation of the positions of the co-located phase centers can be interpreted as specific displacements of the receiver array [7],[8]. The more overlapping phase centers that exist, the easier it is to estimate the parameters of the motion. The important requirement of this technique is that there **must be overlap** of phase centers from sequential pings [5].

But there is a completely different way to approach the problem of sway and yaw estimation which we have dubbed "Displaced Ping Imaging Autofocus" (DPIA) and is more akin to the Map Drift SAR algorithm than RPC. With a multiple receiver array SAS, it is possible to compute a low angular resolution image from a reflecting object within

This work was partly sponsored by the Department of the Navy, NAVSEA Coastal Systems Station, Panama City, Florida as Grant N61331-02-1-G003

the sector of the swath illuminated by a single pulse of the transmit beam. Provided the individual elements of the receiver array have a broad beam-width response, the low-resolution image computed from a second ping will have considerable overlap with the low-resolution image computed from the first ping. Providing that nothing moves except the SAS platform (and again we are ignoring temporal

decorrelation caused by medium fluctuations), these two images have a high degree of overlap and so redundancy. Since we have a high degree of redundancy, there is a high degree of correlation in the two low-resolution images even if there is no overlap of the phase centres (and so little or no redundancy and correlation in the raw data). Consequently we now have a way to estimate the differential yaw and differential sway by cross correlating the two low-resolution images. Now the SAS is free to travel at the maximum allowable speed where there is no overlap of any phase centers and little if any correlation between the echoes at phase centers from adjacent pings. The only requirement of this proposed technique is that there **must be overlap and correlation in the individual low-resolution images** computed from sequential pings; a technique similar to this has been proposed before in [9] and more recently but without details in [10].

As designed for single-receiver SAR systems, the Map Drift algorithm has a similar approach to the problem of sway across the aperture as a function of along-track position. The total aperture is divided into a number of sub-apertures (which may or may not have overlapping sections)and a number of low-resolution images are formed using the echos appropriate to each sub- aperture. The images are usually arranged onto Cartesian coordinate system. By cross-correlating adjacent low-resolution images, a polynomial (with the exception of the constant and first-order coefficients which do not effect the image quality, only the image location) describing the differential sway history along the track can be determined [11]. In the first application of the original Map-drift technique, the aperture was divided into two equal but non- overlapping sub-apertures and two images created with a theoretical along-track resolution about half that of the full aperture. There was sufficient information in the cross-correlation of these two images to determine a parabolic departure (i.e., effectively a second-order defocus term) from a straight flight (cf. tow) path. As the total aperture was divided into smaller and smaller sub-apertures, the higher the order of the polynomial fit to the unknown sway history. The limit to this technique with a single-receiver SAR would be when the number of aperture samples in any one sub-aperture are too small to form a recognizable "image". With DPIA we propose here, it is more straightforward since the most convenient sub-aperture to employ is the multi-receiver physical array itself. All that is required is that the number of receivers in the physical array of hydrophones is sufficient to form an image — here we are assuming the physical array is well-filled as has no gaps between any of the individual elements. Clearly the more hydrophones in the physical array, the better the image and the more precisely the cross-correlation can determine the differential sway between pings. In addition since all the hydrophones are mounted on a straight keel, the proposed DPIA algorithm has the ability to determine the differential yaw of the towfish as well as its differential sway. This is a significant extension to the original single-receiver Map Drift algorithm.

The basis for our initial simulation is a side-looking sonar with specifications close to those of the slow speed SAS recently built by Northrop-Grumman [12].

II. Multiple-receiver SAS

The sonar system model one transmitter projector at the centre of rotation and has H receiving hydrophone elements all aligned in the direction of travel where each hydrophone has an integer index $h \in [0, H-1]$. The position of the h^{th} hydrophone element relative to the centre of rotation around the sonar's long axis is $d = (h - H/2)\Delta d$ with Δd the separation of the hydrophone element centres The data collected by this new multi-hydrophone sonar is now

$$ss(t,u,d) \;=\; \int_x \int_y ff(x,y) \cdot a(t,x,y-u-d) \odot_t \qquad (1)$$
$$\wp\!\left(t - \frac{1}{c}\sqrt{x^2+(y-u)^2} - \frac{1}{c}\sqrt{x^2+(y-u-d)^2}\right) dx\, dy.$$

For reasons that will be apparent later, we often need to re-order this 3-dimensional matrix into a series of 2-dimensional matrices *viz*

$$ss(t,u,d) = ss_p(t,d).$$

where p is the ping index and $u = p\Delta U$ with ΔU the distance travelled between pings.

III. Yaw estimation using DPIA

The traditional technique for yaw estimation from multiple hydrophone SAS is to ensure sufficient overlap in the projector/ hydrophone phase centres from adjacent pings that all but the roll and slant-range heave degrees of freedom can be estimated using the DPCA algorithm. Clearly if only sway and yaw are required, then the amount of phase centre overlap can be reduced but some overlap in the phase centres is always required for DPCA. What we suggest here is that instead of correlating the raw data from each ping to determine the sway and yaw, we compute individual images from each ping and then determine the sway and yaw from the overlap of the low-resolution images. Since the beamwidth of the individual hydrophone elements covers a very much broader along-track distance than the distance moved between pings, there is always considerable overlap of the images even when travelling at the maximum allowable speed as set by the spatial sampling theorum.

We have a number of options in computing the individual low resolution images from each ping. The images can be computed on a cartesian grid giving $\widehat{ff}_p(x, y)$ where the origin of y can be world-centred or ping-centred. However since images from adjacent pings are to be cross-correlated to estimate sway (a cross-track distance in x) and yaw (an angle θ), the most appropriate image is in fact $\widehat{ff}_p(x, \theta)$ where the origin of x, θ coordinates lies at the centre of rotation of the towfish at ping p. Although a perfect matched filter can be determined for each point in x and θ, there is no really efficient way to process blocks of data in one inverse-filtering operation.

A more efficient process is based on individual ping-centred, polar images $\widehat{ff}_p(r, \theta)$ which can be computed with Fourier-based techniques. There is some range migration in off-axis reflectors between the two ping images, however, this can be accomodated by a small decrease in range resolution if this causes any problems.

IV. Single-ping polar imaging

Taking the data from a single ping, $ss_p(t, d)$, we can reconstruct a limited-resolution, ping-centred polar image $\widehat{ff}_p(r, \theta)$ using any convenient azimuth compression algorithm that results in a geometrically correct image in ping-centred polar r, θ coordinates.

$$\widehat{ff}_p(r,\theta) \approx \iint ss_p(t,d) \cdot \wp\left(t - \frac{1}{c}\left[2r - r_0 + \sqrt{r_0^2 + 2r_0 d \sin\theta + d^2}\right]\right) dt\, dd \qquad (2)$$

but this only valid for narrow swath imaging when $r \approx r_0$ A simpler and faster transformation can be used to compute the individual ping-centred polar image $\widehat{ff}_p(r, \theta)$ from $ss_p(t, d)$. The basis for this simpler Fourier-based transformation is

$$\begin{aligned} \widehat{ff}_p(r,\theta) &\approx \mathcal{R}_{t,\,k_d}\{\mathcal{F}_d\{ss_p(t,d)\}\} \qquad (3) \\ &= \mathcal{R}_{t,k_d}\{sS_p(t,\,k_d)\} \end{aligned}$$

where the $\mathcal{R}\{\cdot\}$ transformation is a coordinate mapping given by $t \Rightarrow 2r/c$, and $k_d \Rightarrow k_0 \sin\theta$ centred on ping p. Note that no interpolation is required for $\mathcal{R}\{\cdot\}$ mapping from t and k_d coordinates into r and θ coordinates but it does rely on the narrowband approximation of $k_d \approx k_0 \sin\theta$.

V. Estimating Differential-yaw

But what if there is a change in towfish yaw between the two images? Clearly each polar image is displaced in angle relative to each other but not in range. Thus by following the process summarised in the flow diagram of fig. 1, the actual angular change required to bring the images into coincidence can be estimated by cross-correlating the two images. Because the rotational centre of the towfish for ping $(p+1)$ and ping p are displaced by the distance moved between pings, the origin of each image is slightly different and the cross-correlation has a range-dependent

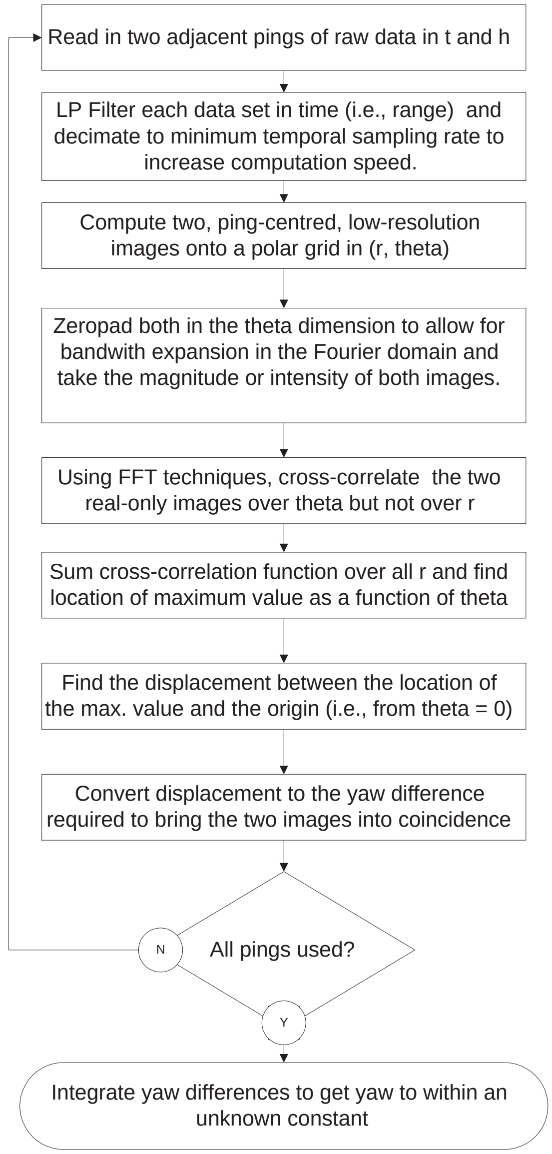

Fig. 1. Basic flow diagram when cross-correlating the image intensities. Cross-correlating the image magnitudes and the complex images follows a similar proceedure with some changes in the zero-padding and finding the maximum value. See the text for more details.

error. By non-symetrical zero padding appropriately before the Fourier into k_d, we can use a common center of polar coordinates

$$cc_p(r,\theta) = |\widetilde{ff}_{p+1}(r,\theta_p) \star_\theta \widetilde{ff}_p(r,\theta_p)|. \qquad (4)$$

The maximum value of $cc_p(r, \theta)$ for each value of r identifies the shift in θ—call this $\theta_p(r)$—required to bring that range of the two ping-centred images into coincidence. Clearly $\theta_p(r)$ is the **differential** yaw of the sonar platform between ping $(p + 1)$ and ping p at range r. Since the differential yaw required is independent of r, a better estimate of the differential yaw can be found by summing

$cc_p(r, \theta)$ over all r,

$$c_p(\theta) = \sum_r cc_p(r, \theta). \quad (5)$$

where the location of the maximum value of $c_p(\theta)$, let us call this θ_c, gives a coarse estimate of the angle required to bring the two images into coincidence. If there is no change in yaw angle between the two images, the maximum value of $c_p(\theta)$ occurs at the origin and so for this situation $\theta_c = 0$.

Cross-correlating the two complex-valued, low-resolution, polar images and finding the location maximum value of the **envelope** gives a coarse but reasonably robust estimation of the "delay" in θ necessary to bring the two polar images into coincidence. A more accurate estimate can be found from the phase of the cross-correlation at θ_c; call this the fine estimate of the "delay" angle θ_f. Since there is a 2π ambiguity in the phase measured at θ_f, this phase estimate must be unwrapped until $(\theta_c - \theta_f)$ is a minimum. As a minor matter of practical detail, even more robust estimators are ones based on the cross-correlation of the real-only **amplitudes** or even the **intensities** of the two ping-centred low-resolution polar images e.g., $|\widetilde{ff}_{p+1}(r, \theta_p)| \star_\theta |\widetilde{ff}_p(r, \theta_p)|$ and $|\widetilde{ff}_{p+1}(r, \theta_p)|^2 \star_\theta |\widetilde{ff}_p(r, \theta_p)|^2$. These are particularly useful where there is a large amount of reverberation or clutter noise and we used this latter correlation to start the whole estimation proceedure, however, care must be taken to zero pad the modulii or the intensity images in the θ direction to account for any spatial bandwidth expansion in θ caused by the non-linear operations. The cross-correlation of the image intensities is shown in the flow chart of fig.1.

VI. Yaw and sway estimation

To test the efficacy of the proposed algorithms, we need to estimate the yaw and sway and then compare it in some meaned squared-error sense to the actual yaw and sway. Firstly we simulate a 32 hydrophone receiver SAS. The centre of rotation (CoR) is considered to pass through the centre of the hydrophone array and the middle of the transmitting projector. The SAS travels at $3.5\,\mathrm{ms}^{-1}$ radiating a $10°$ beam of sound at a centre frequency of 100kHz with a pulse bandwidth of 20kHz and repeating every 0.29 s. The tow-velocity of the SAS is such that there is **no phase centre overlap** and the leading-most phase centre of one ping is adjacent to the trailing-most phase centre of the next ping. The received data from each of the 32 hydrophone receivers is well over-sampled, demodulated to complex baseband and decimated to a sampling frequency of 30kHz. The first image shown in fig. 2. This displays the magnitude of the raw data (unprocessed other than demodulated to complex base-band and pulse compressed in range) from just one hydrophone receiver detected from a rectangular block object surrounded by point reflectors and immersed in random uncorrelated noise. The effect of random sway on the unprocessed image is quite noticable. The yaw errors and sway errors are ploted in fig. 3 and fig. 4. Since the actual sway and yaw used to create the raw data are known, they can be corrected for in the image reconstruction algorithm (in this case a modified form of the wavenumber algorithm) and the diffraction-limited image intensity available for visual comparison.

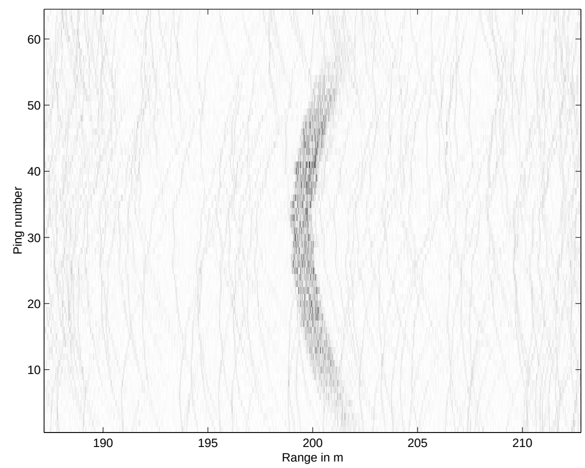

Fig. 2. Unprocessed raw data with non-zero yaw and sway included

Now for the test of the yaw and sway estimation procedure. The data from all 32 receivers for any two sequential pings is applied to the single ping imaging algorithm and the yaw differences estimated from the θ cross-correlation of the intensity of the two images. This is combined with the sway differences estimated from the r cross-correlation of the same two images. Now the difficult step is to estimate the sway and yaw from the measured sway differences and measured yaw differences since there is no unique way of separating constant yaw from linear sway. Once this procedure has been completed, we can compare the actual sway and yaw that was inserted into the data collection simulation with the estimated sway and yaw determined from the unprocessed raw data alone. Figure 6 shows comparison of the yaw and yaw estimates both with the means

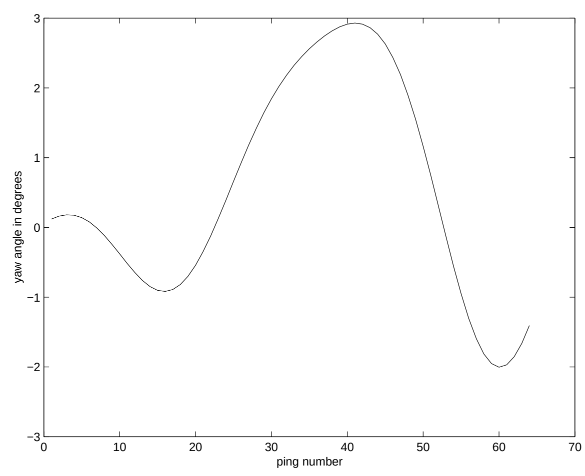

Fig. 3. Yaw angles used to distort the collected data. Note the non-zero mean.

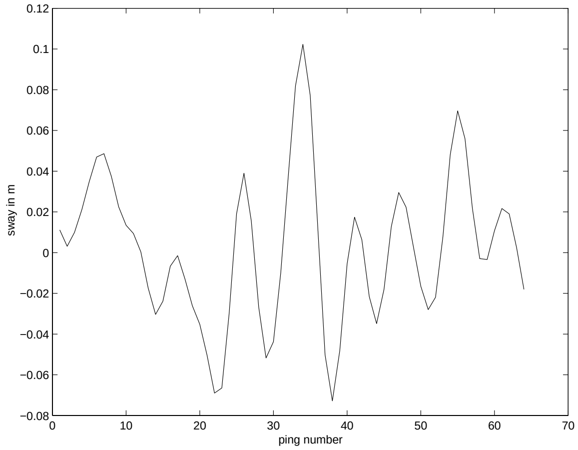

Fig. 4. Sway displacements used to distort the collected data.

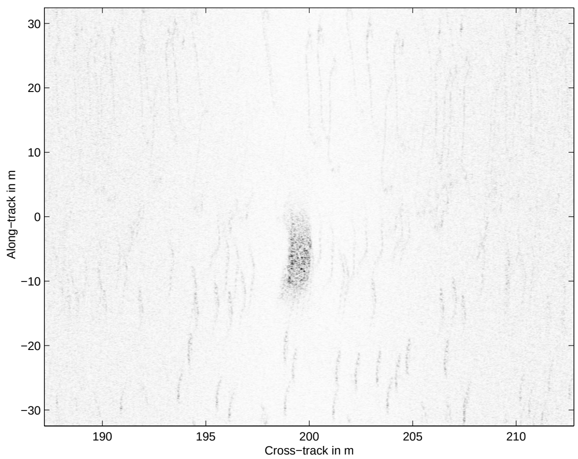

Fig. 5. Processed image showing effect of uncorrected yaw and sway

removed. Figure 3 should be compared with fig.6 to see the amount of constant yaw offset. The unknow mean yaw will be compensated for as a constant linear sway in the sway estimation process. Since no algorithm based on detecting yaw and sway *differentials* can distinguish between a constant yaw offset and a linear trend in sway, we believe the decision to assume the estimated yaw is zero mean is justifiable.

Finally it remains to be seen just how effective the DPIA algorithm is in estimating the yaw and sway and how the image is improved using these estimates. Comparing the magnitude of the reconstructed image shown in fig. 7 to the diffraction-limited image magnitude shown in fig. 8, it can been seen that the image is very much closer to the diffraction-limit than the image using no correction at all, fig. 5, but it is clear that there is still a little way to go to get to true diffraction-limited image fig. 8. It is also clear that a strong cultural (*i.e.*, man-made) target appears to bias the results so that images of areas including such targets are not as good as images of targets fields comprising of nothing more than a selection of almost- equal intensity

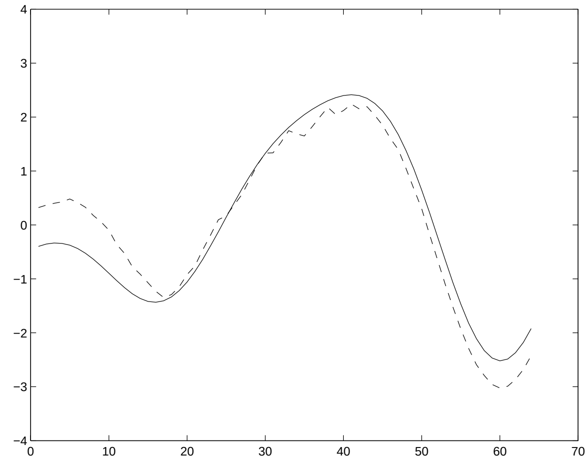

Fig. 6. Yaw estimates in degrees (dashed line) compared to actual yaw (solid line) both with means removed

point reflectors.

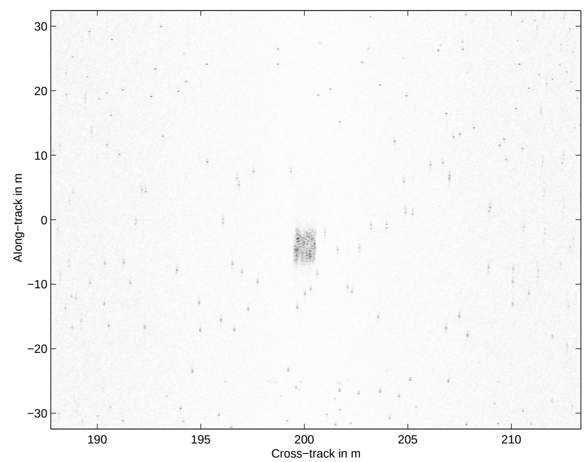

Fig. 7. Reconstructed image corrected for estimated yaw and estimated sway

VII. Conclusions

The reconstructed images created using a hydrophone array SAS are almost always impaired by unknown random yaw and sway. Consequently autofocus algorithms need to be able to estimate the random yaw and sway histories reasonably accurately. By cross-correlating two limited-resolution, ping-centred images computed using data collected from two adjacent pings, we can estimate the differential yaw and sway that occured between the two pings. With suitable integration over the full set of recorded echoes, we can estimate overall yaw histories down to $1/10°$ and sway histories down to a fraction of a wavelength (at least in computer simulations). This can be done very efficiently by computing the low-resolution, single-ping images onto a polar r, θ (rather than a Cartesian x, y) grid which can be slightly modified to allow for the origin offset of the

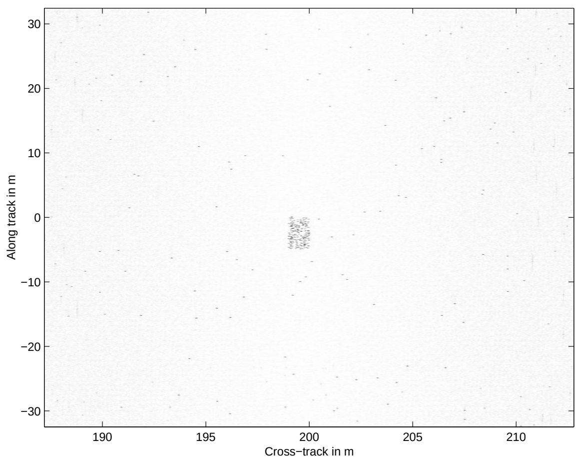

Fig. 8. For comparison diffraction-limited image after the actual yaw and sway displacements have been corrected

small distance moved between pings. The important aspect of this yaw and sway estimation process is that there is no requirement for overlapping phase centres and the SAS can travel at its maximum allowable speed thus also maximizing the available mapping rate.

Target fields that include strong targets need to be handled carefully since their presence appears to bias the motion estimates and we have also noticed this in single hydrophone SAS sway estimators based on the unprocessed echos such as shear averaging [13], [14], [15].

Since the accuracy of the our combined yaw and sway estimation autofocus algorithm frequently exceeds that of many navigation instruments, an inverted consideration of sub-marine operations is possible which may be extremely valuable for AUVs. Instead of using costly, on-board, navigation instruments (e.g., fiber-optic INS, inclinometers and accelerometers) to estimate motion parameters then subsequently used to correct imperfect images, perhaps we should be using SAS autofocus techniques to estimate key motion parameters subsequently used to correct imperfect navigation. Although this may seem a departure from current thinking, we could consider the multiple-hydrophone receiver SAS as no more than a very sophisticated multibeam, Doppler velocity profiler. Thus it could be possible that sometime in the future, all AUVs will be deployed with an array SAS on board not for imaging, but for navigation.

References

[1] Gough, P.T., and Hawkins, D.W., "Imaging algorithms for a strip-map synthetic aperture sonar: Minimizing the effects of aperture errors and aperture undersampling," *Oceanic Engineering IEEE J.*,1997, **22**(1), pp. 27–39.

[2] Chevillon, D., Rastello, T. and Vray, D., "A Fourier-based motion estimation approach for wide band sythetic aperture sonar," in *Oceans '98 Conference Proc.*. IEEE, 1998, **3**, pp. 1671–1675.

[3] Shippey, G., Ulriksen, P. and Liu, Q., "Wideband swath bathymetry, SAS autofocus and underwater navigation fixes: three related problems in echo/image correlation," in *IEE Sonar Signal Processing Conference*, Weymouth, December 1998.

[4] Banks, S.M., and Griffiths, H.D., "Imaging and motion estimation for synthetic aperture sonar based on Fast Factorised Back-Projection," ECUA'2002, 24-27th June 2002, Gdansk, Poland.

[5] Bellettini, A. and Pinto, M., " Experimental investigation of synthetic aperture sonar micronavigation," in *Proc. 5th European Conf. on Underwater Acoustics*, ECUA'2000, Lyon, France, pp.445-450.

[6] Christoff, J. T., " Motion-compensated high frequency synthetic aperture sonar", *J. Acoust. Soc. Am.*, 1998,**l**, pp.2950

[7] Pace, N.G., Bergen, O. and Pinto, M., "Some aspects of shallow water fluctuations on SAS performance", in *Stochastic volume and surface scattering: recent developments in underwater acoustics*, *Proc. Inst. Acoustics*, 1999, **21** (9), pp.67—76.

[8] Pautet, L,Pouliquen, E. and Crawford, A., "Experimental study of fluctuations in coherent backscattering", in *Proc. 6th European Conf. on Underwater Acoustics*, ECUA'2002, 24-27th June 2002, Gdansk, Poland, , pp.157—162.

[9] Douglas, B.L. and Lee, H., "Synthetic-aperture imaging with a multiple element receiver array", *IEEE Int. Conf. on Acoustics, Speech & Sig. Proc.*,1993, April, **5** , pp.445—448.

[10] Groen, J. and Sabel, J.C., " Interaction between autofocussing and synthetic aperture processing: a study based on simulations and experimental rail data", in *Proc. 6th European Conf. on Underwater Acoustics*, ECUA'2002, Gdansk, Poland, 24-27th June 2002, pp.235— 240.

[11] Brown, W.D. and Ghiglia, D.C., " Some methods for reducing propagation-induced phase errors in coherent imaging systems. I Formalism ", *Opt. Soc. Am., J.*, 1998, **5** (6), pp.924—940.

[12] Keeter, H., "Navy awards Northrop Grumman $3.5 million synthetic aperture sonar contract," *Defense Daily*, March 2002, **209**(3).

[13] Callow, H.J., Hayes, M.P. and Gough, P.T., "Wavenumber domain reconstruction of SAR/SAS imagery using single transmitter and multiple-receiver geometry," *Electronics Letters*, March 2001, **38**(7), pp. 336–337.

[14] Callow, H.J.,Hayes, M.P. and Gough, P.T., " Noncoherent autofocus of a single-receiver broad-band synthetic aperture sonar imagery", *IEEE Oceans 2001*, Sept. 2001, Honolulu, Hawaii, pp.157—162.

[15] Johnson, K.A., Gough, P.T. and Hayes, M.P., "A method of estimating the sub-wavelength sway of a sonar towfish", *Oceanic Engineering, IEEE J.*, 1995, **20** (4), pp. 258—267.